At What Time of Day Do Daily Extreme Near-Surface Wind Speeds Occur?

Robert Fajber, Adam H. Monahan, & William J. Merryfield

May 2014

At What Time of Day Do Daily Extreme Near-Surface Wind Speeds Occur?

ROBERT FAJBER AND ADAM H. MONAHAN

School of Earth and Ocean Sciences, University of Victoria, Victoria, British Columbia, Canada

WILLIAM J. MERRYFIELD

Canadian Centre for Climate Modelling and Analysis, University of Victoria, Victoria, British Columbia, Canada

(Manuscript received 23 May 2013, in final form 14 February 2014)

ABSTRACT

The timing of daily extreme wind speeds from 10 to 200 m is considered using 11 yr of 10-min averaged data from the 213-m tower at Cabauw, the Netherlands. This analysis is complicated by the tendency of autocorrelated time series to take their extreme values near the beginning or end of a fixed window in time, even when the series is stationary. It is demonstrated that a simple averaging procedure using different base times to define the day effectively suppresses this ''edge effect'' and enhances the intrinsic nonstationarity associated with diurnal variations in boundary layer processes. It is found that daily extreme wind speeds at 10 m are most likely in the early afternoon, whereas those at 200 m are most likely in between midnight and sunrise. An analysis of the joint distribution of the timing of extremes at these two altitudes indicates the presence of two regimes: one in which the timing is synchronized between these two layers, and the other in which the occurrence of extremes is asynchronous. These results are interpreted physically using an idealized mechanistic model of the surface layer momentum budget.

1. Introduction

Near-surface winds over land are known to undergo a marked diurnal cycle under clear-sky conditions, associated with the diurnal cycle in near-surface stratification (e.g., Barthelmie et al. 1996; Dai and Deser 1999; Arya 2001; He et al. 2013). For example, the diurnal cycles of the mean wind speed at six altitudes from 10 to 200 m (and separated by season) observed at the 213-m-tall tower at Cabauw, the Netherlands, are presented in Fig. 1 (these data are described in more detail in section 2). In each season, the mean vertical shear of the wind speed is weaker during the day and stronger at night; this diurnal cycle is most pronounced in April–June and July–September. In all seasons, the strongest mean wind speed in the bottom few tens of meters at Cabauw occurs during midday, while the strongest mean wind speed above that occurs at night. These cycles follow the canonical picture of fair-weather boundary layer evolution (e.g., Arya 2001; Stull 1997). Mean wind speeds below about 50 m tend to be largest (and wind speeds above about 100 m to be smallest) when the boundary layer is unstable and convectively mixing higher-momentum fluid from aloft with lower-momentum fluid from near the surface. At night the near-surface air becomes stably stratified and largely decouples from the mixed (but no longer actively mixing) residual layer above. The reduced vertical transport of momentum causes the near-surface winds to be slowest at night, on average. This decoupling also allows the residual layer to undergo inertial oscillations caused by the release from surface drag (e.g., Baas et al. 2009, 2010; van de Wiel et al. 2010); the resulting low-level jets (LLJs) are responsible for the large average wind speeds aloft. In fact, not only the mean, but the entire probability distribution of near-surface wind speeds displays a marked diurnal cycle (Monahan et al. 2011; He et al. 2010, 2012, 2013). In addition to these diurnal variations associated with local dynamical processes, variability in the pressure gradient force associated with mesoscale and synoptic-scale systems can also produce wind speed extremes.

While the diurnal evolution of the near-surface wind speed probability distribution has been studied in some

Corresponding author address: Adam Monahan, School of Earth and Ocean Sciences, University of Victoria, P.O. Box 3065 STN CSC, Victoria, BC V8W 3V6, Canada.
E-mail: monahana@uvic.ca

DOI: 10.1175/JCLI-D-13-00286.1

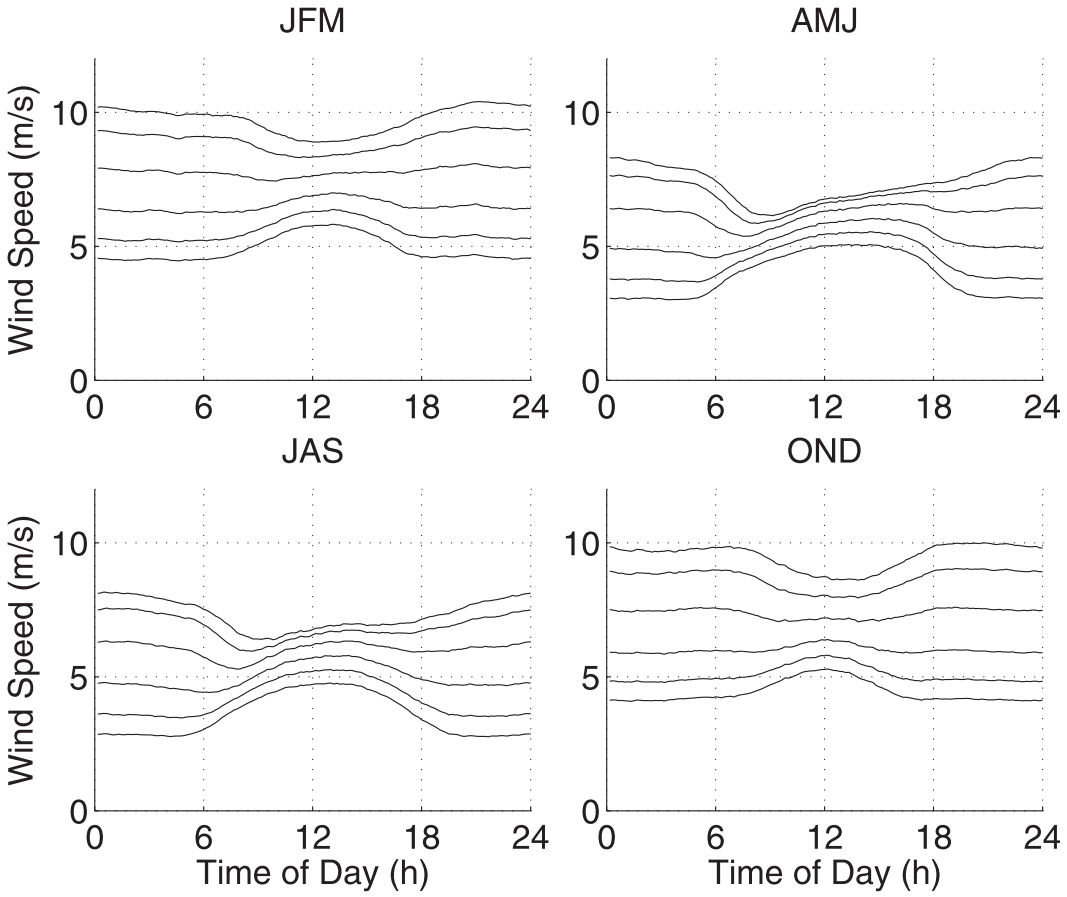

FIG. 1. The observed mean diurnal cycles of wind speed at Cabauw, at altitudes of 10, 20, 40, 80, 140, and 200 m (corresponding to the lowermost to uppermost curves, respectively) for each of the four seasons JFM, AMJ, JAS, and OND. The averages are calculated using data from 1 January 2001 to 31 December 2011.

detail, the diurnal cycle of wind speed extrema has received less attention. In particular, the timing of the strongest wind speeds at different altitudes over the course of the day has not been investigated by previous studies. An understanding of the timing of near-surface wind speed extrema is particularly useful from the perspective of wind power. Times of fastest wind speed correspond to times of greatest wind power density, although if the speed exceeds the cutout wind speed of a turbine this power cannot be extracted (e.g., Burton et al. 2011). Similarly, the occurrence of speed extremes at different altitudes at different times will modulate the magnitude of the vertical wind shear, which if large enough can cause the blades of a turbine to experience potentially damaging torques. Knowing when these extremes are likely to occur at a single or several altitudes is of practical relevance to the management of the wind energy resource. Further motivating the study of extreme winds is the fact that they can result in hazards to the natural and built environment.

In this study, we will consider the timing of daily near-surface wind speed extrema using a long record (11 yr) of temporally high-resolution (10 min) observations between 10 and 200 m from the 213-m-tall tower at Cabauw, the Netherlands. These data are described in detail in section 2. The timing of daily maximum wind speeds is expected to be different at different altitudes, depending on the relative contributions of buoyantly driven mixing processes, LLJ phenomena, and large-scale forcing in producing these extremes. Our methodology for computing the timing of extremes is simple: within time windows corresponding to each 24-h day, we find the maximum wind speed at a given anemometer altitude and record the time at which it occurs. As we will discuss in section 3, this approach to finding the timing of daily extremes is complicated by the tendency of autocorrelated time series to take their extrema at the beginning or end of fixed windows in time, if the autocorrelation time scale is similar to or longer than the window length. After presenting a brief discussion of the

origin of this "edge effect," we will describe an averaging strategy to minimize it and isolate the intrinsic, physically driven nonstationarity of the timing of daily wind extremes. The edge effect and our approach taken to suppressing it are features of the extrema timing of any autocorrelated time series in a fixed window and so these results extend to the timing of the extremes of any climate variable (e.g., wind shear, temperature, precipitation) or time window (e.g., weekly, monthly). In section 4, we will investigate the physical mechanisms controlling the timing of wind speed extremes using an idealized stochastic model of the boundary layer momentum budget adapted from one presented in Monahan et al. (2011). A discussion of the results and conclusions follow in section 5.

2. Data

The wind data considered in this study were obtained from the Cabauw Experimental Site for Atmospheric Research (CESAR), which maintains a 213-m-tall meteorological tower located at 51.971°N, 4.827°E at Cabauw, the Netherlands. A description of the tower is given in van Ulden and Wieringa (1996); up-to-date information and the available data are described online (http://www.cesar-database.nl/About.do). Wind speeds and directions are measured at heights of 10, 20, 40, 80, 140, and 200 m above the surface. Validated observations for 10-min averaged wind speed data from 1 January 2001 to 31 December 2011 were used in this study (downloaded from http://www.cesar-database.nl). We will consider the variability of these winds within individual months, as well as in four seasons: January–March (JFM), April–June (AMJ), July–September (JAS), and October–December (OND). We also will make use of hourly surface geostrophic wind data from 1 January 2001 through 31 December 2011, which were provided by Fred Bosveld at The Royal Netherlands Meteorological Institute (KNMI). These data are based on a two-dimensional polynomial fit to surface pressure observations within 75 km of Cabauw, from which the gradient is calculated.

3. Timing of daily maximum near-surface wind speeds

a. *The raw distribution of daily maximum timing*

To compute the timing of the daily maximum wind speed at a given level, the data were divided into individual days, defined as 24-h windows starting at the base time t_0 (which can range from 0000 through 2350 in 10-min increments). Within each of these windows, the maximum wind speed and the time at which it occurred were found. Frequency distributions of these maximum speed values and occurrence times over all 24-h periods were then computed. Note that the timing of extremes within individual days is a feature that is local to (day-long) subsets of the time series, and cannot be characterized by a global analysis of the entire time series such as a Fourier analysis (in contrast to the mean diurnal cycle; cf. Dai and Deser 1999).

Frequency distributions of the magnitude and timing within the day of daily wind speed maxima for each month and altitude and using a base time t_0 of 0000 are presented in Figs. 2 and 3, respectively. As would be expected from the mean shear profile of the lower atmosphere, the daily maximum wind speeds are larger at higher altitudes than at lower altitudes. Similarly, because large-scale synoptic variability is more intense in winter, the distribution of daily extreme winds extends to larger speed values during the winter than the summer. Figure 3 indicates that between 10 and 40 m, extremes are most likely to occur during the day, such that they are most common in late morning and early afternoon in spring through autumn (with this enhanced probability extending into the late afternoon in summer). At 140 m and above, wind speed extremes are more likely to occur at night—particularly in a narrow band of high probability centered at midnight, corresponding to the base time t_0.

While this band is most evident at 140 and 200 m, such a narrow band of high probability centered at t_0 is found at all levels (particularly during the winter). Frequency distributions of the timing of JAS 10-m daily wind speed maxima are shown in Fig. 4 for base times t_0 between midnight and 2300. For all base times, there is a broad maximum in the timing of wind speed maxima centered at approximately 1300. Superimposed on top of this is a narrow peak centered at the base time t_0. As the base time is moved to later in the day, this narrow peak moves with it across the distribution of the timing of maxima. The amplitude of this narrow peak varies also with the base time, such that it is largest when it coincides with the center of the (t_0 independent) broad midday maximum. Similar results are observed for the timing of maxima at other levels (not shown). Note that unlike the distribution of the timing of wind speed maxima, the distribution of the magnitude of the maxima is independent of the base time t_0.

b. *Edge effects in autocorrelated time series*

The narrow peak in the timing of daily extrema centered around the base time t_0 results from the tendency of autocorrelated time series (of sufficiently long autocorrelation time) to take their extrema at the beginning or the end of any specified window in time. We will refer

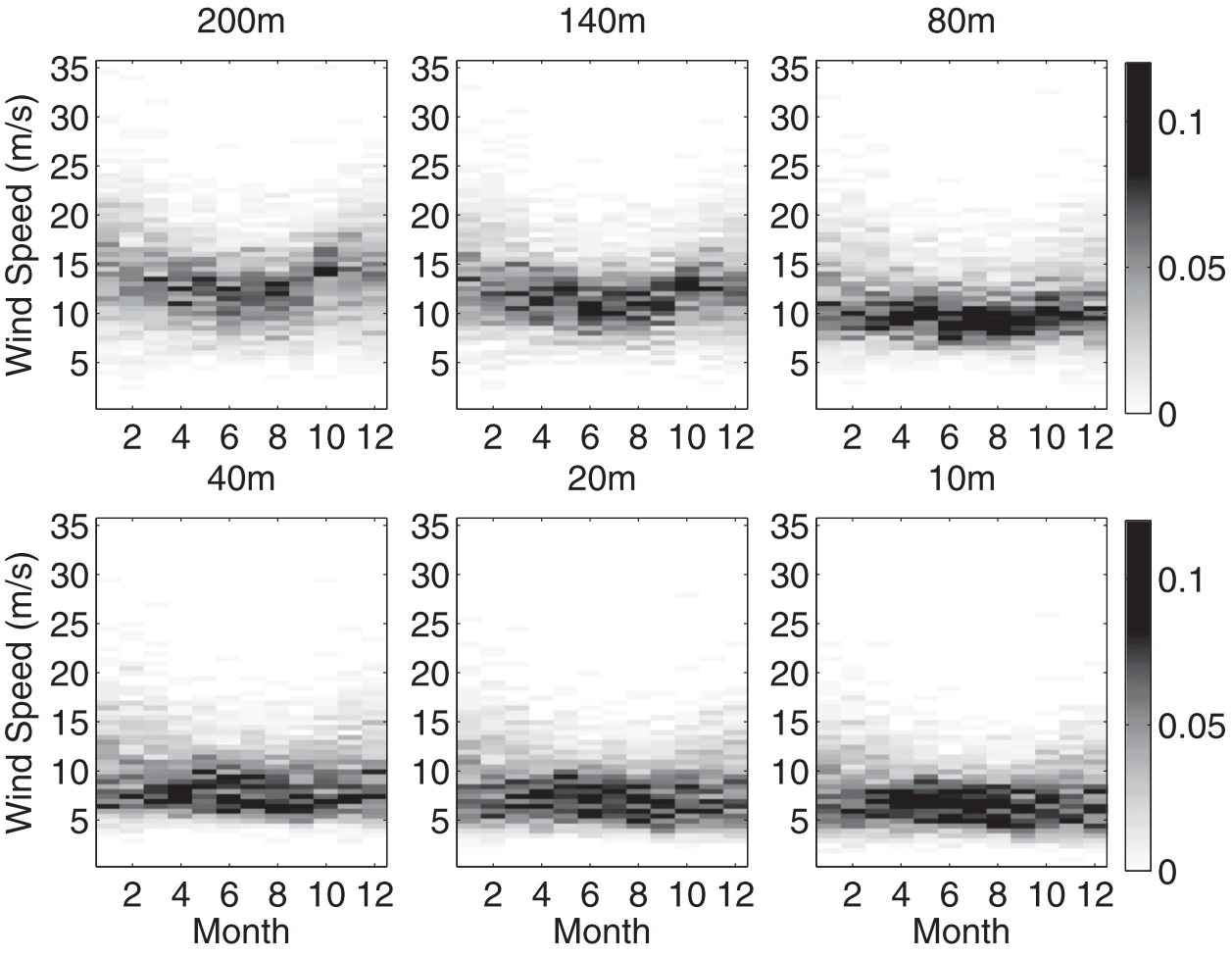

FIG. 2. Frequency distributions of daily maximum wind speeds at Cabauw, for each month and anemometer altitude. These distributions are independent of the base time t_0.

to this aspect of the statistics of the timing of extrema as the edge effect. Near-surface winds are autocorrelated from one day to the next (Fig. 5) because the driving large-scale pressure gradient force evolves slowly on multiday time scales. The influence of local, diurnally evolving boundary layer processes is weaker (relative to the large-scale influence) during JFM than during other seasons. Accordingly, the JFM autocorrelation function decays more slowly than in other times of the year, with little evidence of a diurnal cycle. In contrast, the marked diurnal cycles in the autocorrelation function in AMJ and JAS demonstrate the enhanced influence of local boundary layer processes (particularly within 20 m of the surface).

The fact that the extrema of autocorrelated time series within specified windows have an enhanced probability near the boundaries of the window—irrespective of the base time of the window—has been recognized previously. Coakley (2000) demonstrated that the warmest day within the week tends to occur at its beginning or end, regardless of which base day is used to define the week, and discussed the origin of this effect in terms of first-order autoregressive [AR(1)] Gaussian processes. A detailed mathematical analysis of this edge effect was recently presented in Samorodnitsky and Shen (2013a,b). We will now present a brief discussion of the origin of the edge effect, in order to motivate the subsequent discussion of strategies to suppress it so as to highlight inherent nonstationarities in the timing of extrema. Before doing so, we note that the results of Samorodnitsky and Shen (2013a,b) admit the existence of stationary stochastic processes for which the distribution of extrema within a fixed interval takes a maximum inside rather than at the ends of the interval. However, the edge effect should be characteristic of all geophysically relevant time series that have smooth autocorrelation functions that decay to zero for large enough lags (although this decay does not need to be monotonic or uniform) and for which the maximum within a given interval is almost surely unique.

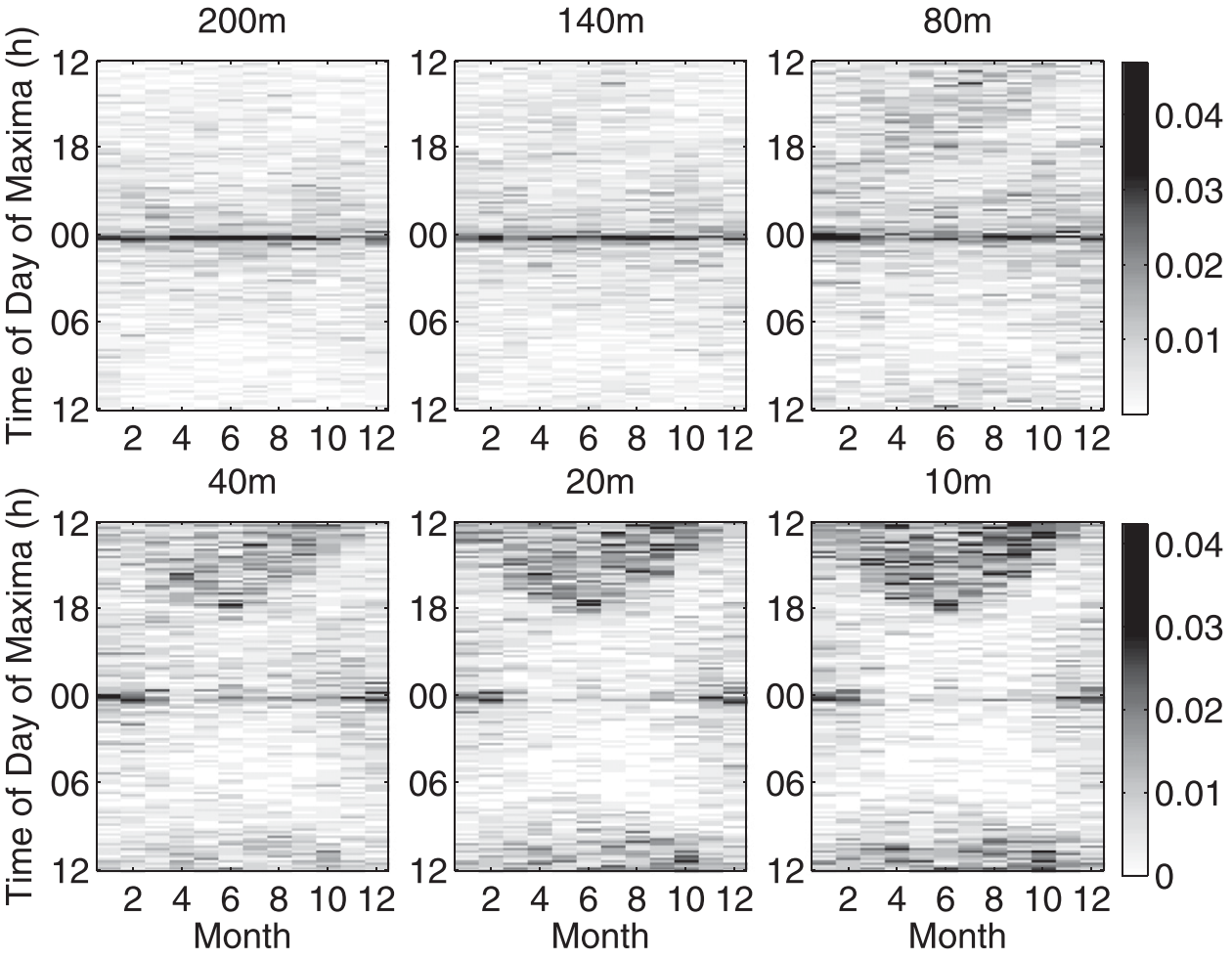

FIG. 3. Frequency distributions of the timing of wind speed maxima over all months at all anemometer heights at Cabauw, for the base time $t_0 = 0000$.

Consider a strictly stationary time series $z(t_n)$ of length NM points, divided into N nonoverlapping, coterminous windows of length M points. In the limiting case that the values of $z(t_n)$ at different times are mutually independent, within any given window each of the M observations is equally likely to be the largest and the distribution of maxima will be uniform across the window. In the opposite limit that the autocorrelation time scale greatly exceeds the width of the window, it is highly likely that the process will be either increasing or decreasing across the window. In this case, the maxima will most frequently occur at the beginning or the end of the window (i.e., near the base time t_0). When the autocorrelation time scale of the process is of the same order of magnitude as the width of the window (as is the case with the wind data under consideration, with 24-h windows), extrema can occur at any point throughout the window but will have an enhanced likelihood at its boundaries (cf. Fig. 6). The temporal invariance of the statistics of the stationary time series is broken by the specification of a window with fixed beginning and end points, resulting in a distribution of the timing of maxima that is generally peaked around the window boundaries.

For a more quantitative investigation of the controls on the edge effect, we will consider synthetically generated time series with statistics that are specified to be qualitatively similar to those of observed wind speeds (nonnegative variables with nonzero autocorrelation time). A simple time series with these features is the amplitude $x(t) = \|\boldsymbol{\eta}(t)\|$ of a realization of the two-dimensional Ornstein–Uhlenbeck process (OUp) $\boldsymbol{\eta}(t)$ with mean zero, variance σ^2, and autocorrelation e-folding time τ. The OUp is particularly convenient to use because its statistics can be simply specified and it is easy to simulate numerically (e.g., Kloeden and Platen 1992; Gardiner 1997). Such a process is described by the stochastic differential equation (SDE)

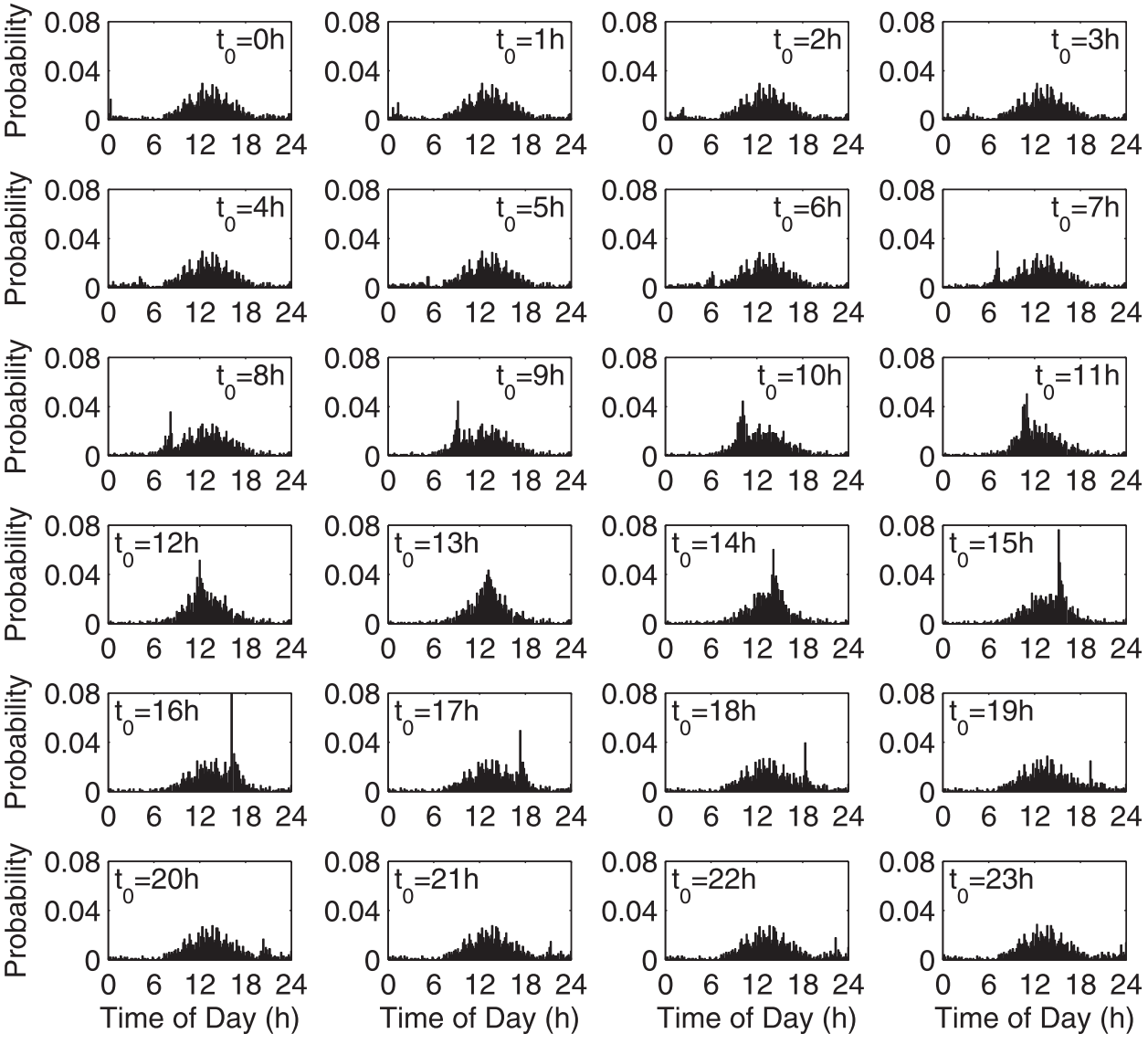

FIG. 4. Frequency distributions of the timing of JAS 10-m daily maximum wind speeds at Cabauw, for a range of base times from $t_0 = 0000$ to $t_0 = 2300$ (as indicated in the panels).

$$\frac{d}{dt}\boldsymbol{\eta} = -\frac{1}{\tau}\boldsymbol{\eta} + \sigma\sqrt{\frac{2}{\tau}}\dot{\mathbf{W}}, \tag{1}$$

where $\dot{\mathbf{W}}$ is a vector of mutually uncorrelated Gaussian white noise processes (e.g., Gardiner 1997). The process $\boldsymbol{\eta}(t)$ is bivariate Gaussian with the stationary autocovariance function

$$\langle \eta_i(s)\eta_j(s+t)\rangle = \delta_{ij}\sigma^2 \exp\left(-\frac{t}{\tau}\right) \tag{2}$$

(where s is the base time for the autocovariance function in the stationary limit, δ_{ij} is the Kronecker delta which equals 1 if $i = j$ but is zero otherwise, and the angle brackets represent averaging). It can be shown (e.g., Monahan 2012, 2014) that the amplitude $x(t)$ is Rayleigh distributed with an autocovariance function given to an excellent approximation by

$$\langle x(s)x(s+t)\rangle = \frac{4-\pi}{2}\sigma^2 \exp\left(-\frac{2t}{\tau}\right). \tag{3}$$

The Rayleigh distribution is a special case of the Weibull distribution, which is often used as an empirical model of the wind speed probability distribution (e.g., Burton et al. 2011; Monahan et al. 2011). A time series of length 30 000 days and resolution $\delta = 1$ min with $\tau = 48$ h was generated using a forward-Euler approximation to the SDE (Kloeden and Platen 1992). As the autocorrelation

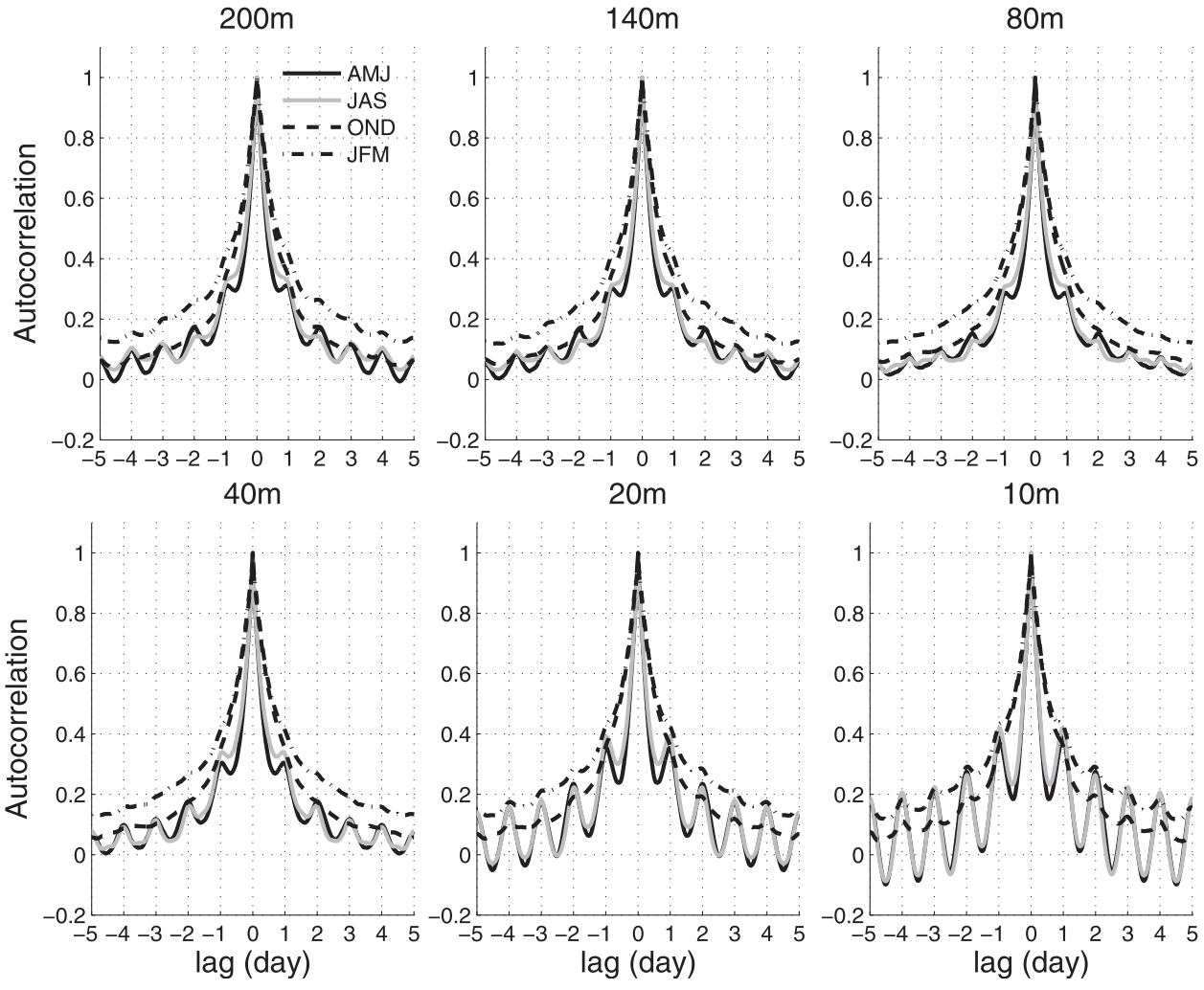

FIG. 5. Lag autocorrelation functions of the observed wind speed at Cabauw for each altitude and season.

e-folding time scale of the wind components is to a good approximation twice that of the speed [Eq. (3)], this value of τ is broadly consistent with the observed wind speed autocorrelation *e*-folding time scales (Fig. 5). The times of daily maxima of x were found from this time series. By construction, these time series are strictly stationary, so there is no intrinsic preference for maxima to occur at any particular time. Frequency distributions of the timing of daily maxima of $x(t)$ for different base times t_0 (Fig. 7) clearly demonstrate the edge effect: the timing distributions of maxima are sharply peaked around t_0 and approximately uniform elsewhere.

Because the edge effect is associated with the enhanced likelihood of autocorrelated series to take their maxima near to the beginning or end of specified windows, the amplitude and width of the associated peak in the timing distribution is sensitive to the resolution of the time series. The realization of $x(t)$ with resolution $\delta = 1$ min discussed above was averaged to resolutions of $\delta = 10$ min and $\delta = 1$ h, and frequency distributions of the timing of daily maxima were computed from these (Fig. 8). As the resolution of the time series becomes coarser, the amplitude of the edge-effect peak around t_0 becomes smaller and broader.

It was noted above that the edge effect peak in the Cabauw wind speed data became larger when the central time t_0 coincided with the broad maximum associated with the intrinsic nonstationarity in the timing of daily maxima. To demonstrate that this amplification in fact results from an interaction between a nonstationarity in the time series and the edge effect, we modified $\boldsymbol{\eta}(t)$ from Eq. (1) to produce a series with a diurnal modulation of its variance:

$$\boldsymbol{\nu}(t) = \{1 - A\cos[2\pi t/(24\text{hr})] + A\}\boldsymbol{\eta}(t). \qquad (4)$$

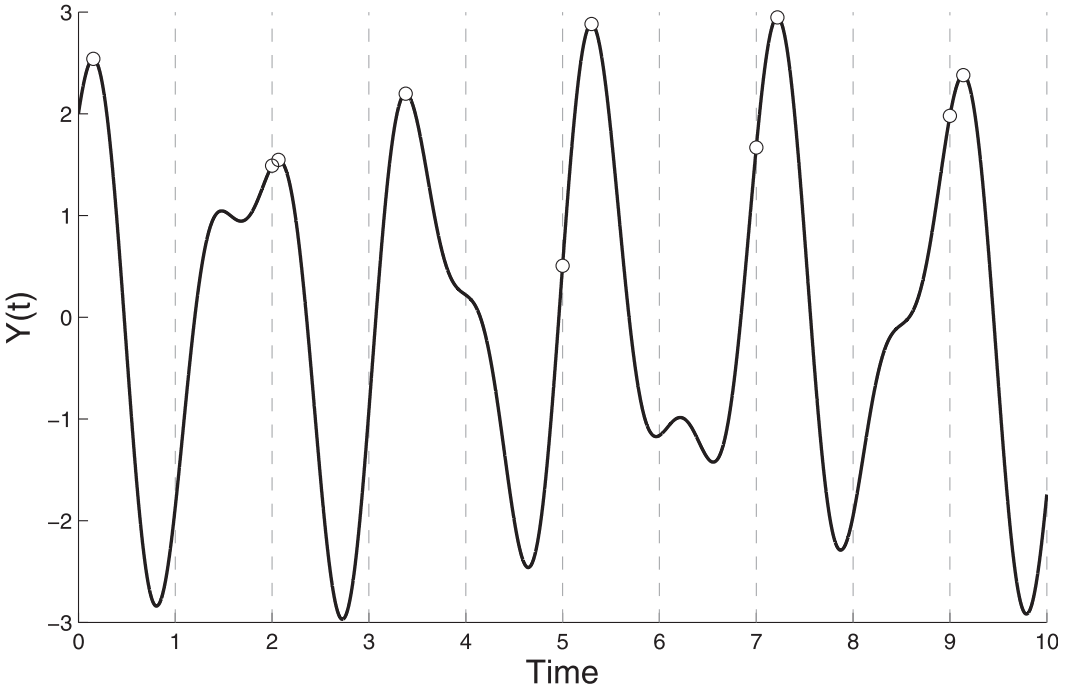

FIG. 6. An illustrative example, adapted from Leadbetter et al. (1983) of the tendency of an autocorrelated time series to take its extrema near or at the boundaries of specified windows if the window length I is sufficiently short. The time series is given by $Y(t) = Y_1(t) + Y_2(t) = A_1 \cos(2\pi t/T_1 - \phi_1) + A_2 \cos(2\pi t/T_2 - \phi_2)$ with $A_1 > A_2$ and $T_1 > I > T_2$. Relative to the window length, the time series $Y(t)$ contains fast and slow components. From visual inspection, it is clear that most of the maxima tend to occur near the edges of the windows. As $T_1 > I$, Y_1 will generally be increasing or decreasing over an entire window; similarly, as $Y_1(t)$ and $Y_2(t)$ have different phases, $Y(t)$ will often take its maximum near or at the boundaries of the window.

The resulting amplitude time series $y(t) = \|\boldsymbol{\nu}(t)\|$ has diurnal cycles in both its mean and standard deviation, with largest values at noon. This intrinsic nonstationarity increases the likelihood of daily maxima to occur in midday. Frequency distributions of the timing of daily maxima of $y(t)$ for $A = 0.25$ (Fig. 9) demonstrate the amplification of the edge-effect peak when it coincides with the peak of enhanced likelihood resulting from the intrinsic nonstationarity.

c. *Filtering the edge effect*

The edge effect is not an artifact of a biased estimator; rather, it is a real feature of the distribution of extremes of autocorrelated time series across specified windows. An inherent nonstationarity in the data, resulting from physically driven modulations of the likelihood of the timing of extrema within specified windows, can be obscured by this edge effect. It is therefore desirable to develop strategies to filter the maxima generated by the edge effect from the maxima associated with the inherent, physically generated nonstationarity.

We will do this by taking advantage of the fact that the position of the edge effect peak is determined by the base time: denoting our window width I, we compute frequency distributions of the timing of maxima for each of the base points ranging from $t_0 = t_{\text{init}}$ to $t_0 = t_{\text{init}} + I - \delta$ in steps of size δ. For example, for the diurnally modulated bivariate OUp amplitude time series $y(t)$ with hourly resolution, we compute $N_{\text{base}} = 24$ separate frequency distributions of the daily maximum $y(t)$ for base times at 0000, 0100, 0200 and so on up to 2300, denoting by f_{ij} the ith bin of the frequency distribution corresponding to the jth base time. Averaging the frequency distributions obtained from the different base times,

$$\mu_i = \frac{1}{N_{\text{base}}} \sum_{j=1}^{N_{\text{base}}} f_{ij}, \tag{5}$$

we suppress the edge effect peak (which is centered at a different position in each frequency distribution) and correspondingly emphasize the intrinsic nonstationarity (Fig. 10). The interaction of the intrinsic nonstationarity with the edge effect is illustrated by the standard deviation of the frequency distributions across different base times:

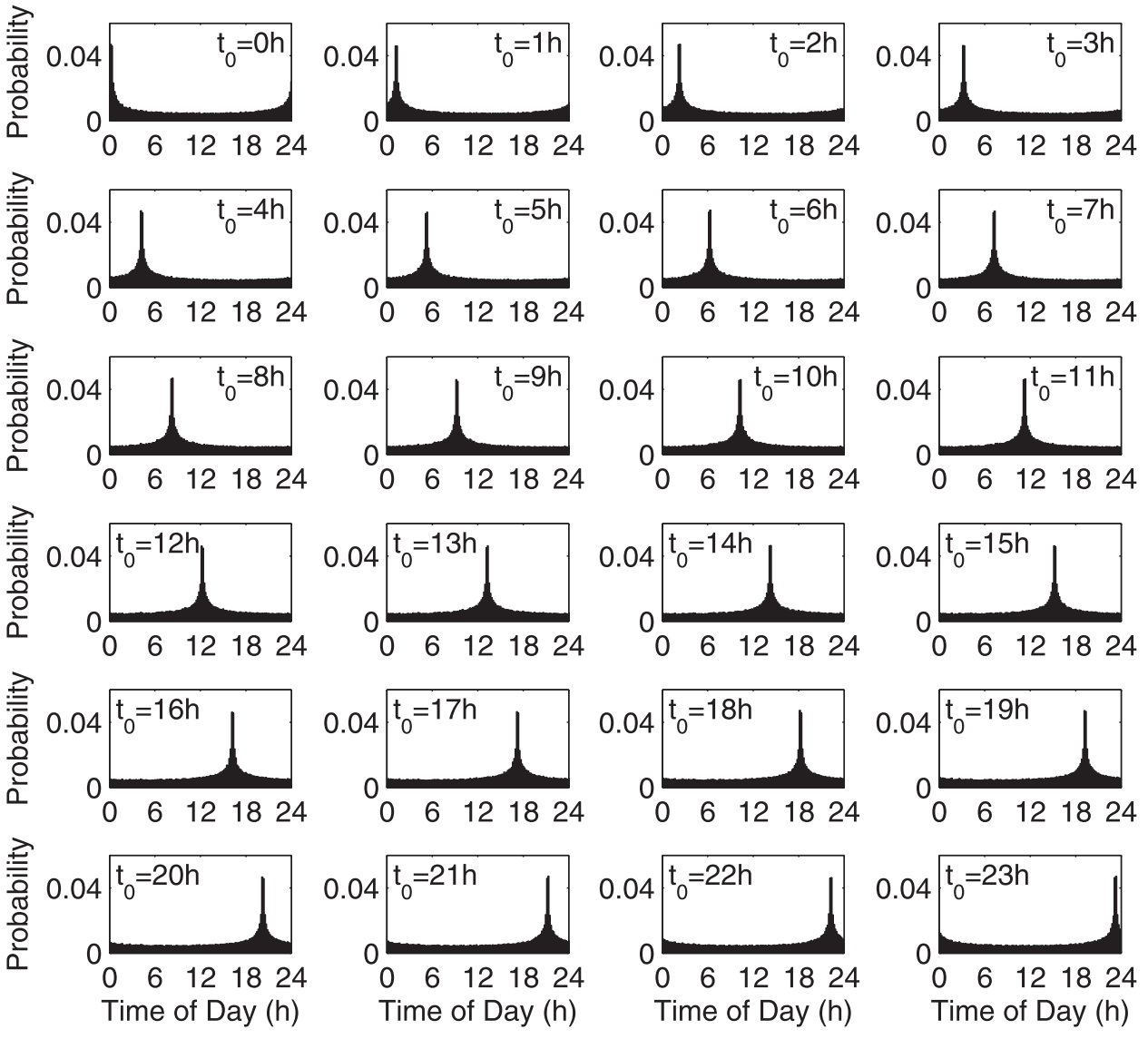

FIG. 7. As in Fig. 4, but for the daily maximum of the magnitude of a bivariate, stationary OUp [Eq. (1)] with autocorrelation time scale τ = 48 h, using a 24-h window and a resolution of δ = 1 min.

$$\sigma_i = \left[\frac{1}{N_{\text{base}}} \sum_{j=1}^{N_{\text{base}}} (f_{ij} - \mu_i)^2 \right]^{1/2}. \quad (6)$$

The frequency distributions computed at different base times differ most from each other at those times when the intrinsic likelihood of maxima is greatest (Fig. 10). Because the interaction between the edge effect and an intrinsic nonstationarity amplifies the edge effect in some places but not others, the averaging procedure will not perfectly separate the two—but it will strongly suppress the signature of the edge effect. When the time series is in fact stationary, the averaging procedure will completely suppress the edge effect, as is demonstrated in an analysis of the stationary time series $x(t)$ (not shown).

Applied to the JAS 10-m and 200-m wind speed data from Cabauw, the averaging procedure clearly demonstrates that daily maximum wind speeds at 10 m occur most often in midday, and only rarely occur in the evenings (Fig. 11, left panels). The timing of peak wind speeds is more evenly distributed across the day at 200 m. While there is a greater probability that maximum wind speeds are achieved in the night, there is a secondary maximum between midday and early evening in the timing of maximum wind speeds at this altitude.

Because the edge effect is strongest when the autocorrelation time scale of the time series under consideration

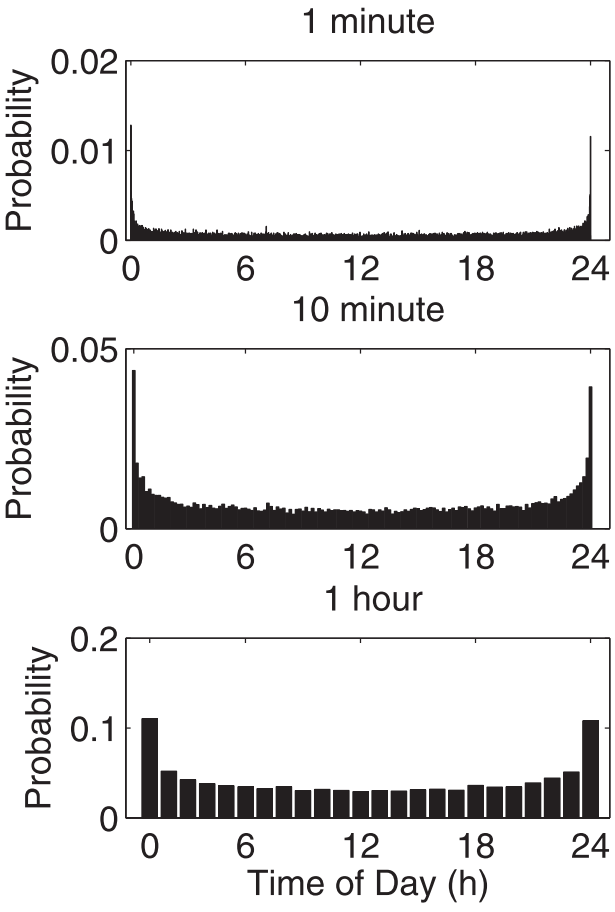

FIG. 8. Frequency distributions of the timing of the maximum daily amplitude of the bivariate OUp [Eq. (1)] for the base time $t_0 = 0$, for different resolutions of the time series: (top) $\delta = 1$ min, (middle) $\delta = 10$ min, and (bottom) $\delta = 1$ h. Note that the values at the extreme left and right are not exactly equal, as the first corresponds to the time range $(0, \delta)$ while the second corresponds to $(24\,\text{h} - \delta, 24\,\text{h})$.

is similar to or longer than the window length I, another way of suppressing this effect is to consider the timing of extrema in longer windows. For example, rather than considering the timing of daily maximum wind speeds, we could consider the timing of maxima within windows of length d days. While this suppresses the edge effect, it also reduces the number of data points used to estimate the timing frequency distributions by a factor of d; the sampling variability of these frequency distributions increases accordingly. The reduction in the number of data points entering the frequency distributions can be offset if instead of considering the largest wind speed within the window, we consider all wind speeds above a specified percentile (and average the frequency distributions across all base times t_0). The analysis presented in the left panels of Fig. 11, using daily windows ($d = 1$ day) with 10-min resolution data, corresponded approximately to considering the 99th percentile wind speeds. When this analysis is changed to consider $d = 2$ days and the 95th percentile winds, the results are smoother, but otherwise much the same as those obtained using the maximum of daily wind speeds (Fig. 11, right panels). Similar results are also obtained for longer windows with lower percentiles, so long as these still represent extreme winds (not shown). If the percentile considered is reduced to the point that it no longer represents extremes, the timing distribution becomes flat.

d. Joint distribution of wind speed extrema at 10 m and 200 m

Having considered the timing of wind speed extrema within a specified time window at individual altitudes, we now consider how the timing of extrema at 10 m relates to those of 200 m. For this analysis, we use an window of $d = 3$ days length, calculate joint frequency distributions of the timing of the 95th percentile winds at 10 and 200 m, and then average these frequency distributions over the base time t_0 (from 0000 to 2350). A window of 3-day width was used because near-surface extreme winds may occur before or after those aloft, and the central day within the 3-day window is symmetrically positioned to account for extremes occurring within the previous or subsequent day.

To estimate the joint distribution of the timing of extrema, events at the two altitudes need to be paired. Because we are considering the 95th percentile wind speeds (rather than the largest value) over the window, there is no unique way for such pairing to be done. Four different pairing strategies were considered:

1) by magnitude: the fastest wind at 10 m within the window is paired with that at 200 m, as are the second-fastest winds, the third-fastest, etc.;
2) by 10-m extreme: the fastest wind at 10 m is paired with all 95th percentile 200-m winds within the window;
3) by 200-m extreme: the fastest wind at 200 m is paired with all 95th percentile 10-m winds within the window; and
4) all pairings: all pairs of 95th percentile 10-m and 200-m winds within the window are considered.

The differences in the joint distributions of the timing of extrema between these approaches are small (not shown). We will focus our attention on the first approach, in which events are paired by magnitude.

The resulting joint distribution for JAS at Cabauw is plotted in Fig. 12. Focusing on the central 24-h period, we see evidence of distinct populations in the timing of extremes. The first of these reflects situations in which wind extremes at 10- and 200-m winds occur separately: the 10-m wind speeds are fastest in midday, whereas the 200-m winds are fastest from just before midnight until

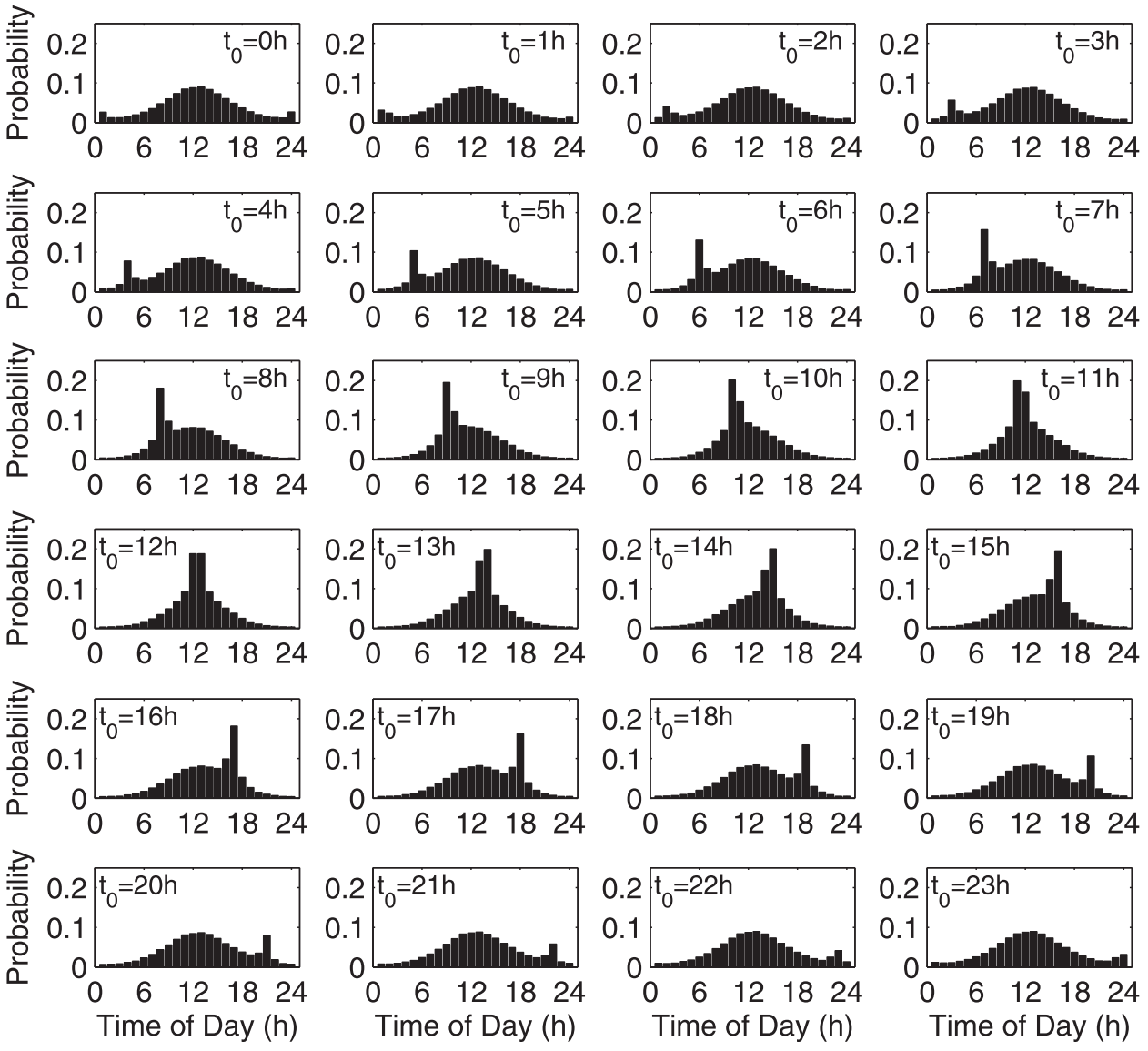

FIG. 9. As in Fig. 7, but for an OUp modulated by a sinusoidal "diurnal cycle" in its variance [Eq. (4)].

early morning. In this "decoupled" population, the occurrences of extremes at the two altitudes are not synchronized. The other population (falling along the diagonal in Fig. 12) corresponds to the simultaneous occurrence of extremes at the two altitudes. This happens most often in the late morning and early afternoon, when the boundary layer is well mixed from 10 m to above 200 m. Extreme winds at the two levels also occur simultaneously at night, when the winds at these levels are often decoupled (but not always; cf. Monahan et al. 2011) due to the formation of a stably stratified inversion layer in the bottom ~50 m. Pairings of points with time separations of greater than 24 h occur, but are much less frequent than pairings of points separated by less than 24 h.

Monahan et al. (2011) found that the joint distribution of wind speeds at 10 and 200 m at Cabauw consists of two regimes: one characterized by a strong wind speed shear (and strongly stable stratification); and the other in which the stratification and wind speed shear are both weak. These two regimes were interpreted as representing uncoupled and weakly coupled states of the nocturnal inversion and residual layers. The two populations in the timing of extremes at night are consistent with these two regimes: when the inversion layer is decoupled from the flow aloft, extremes at 200 m can occur without any influence on surface winds. In contrast, when the layers are coupled, extremes at the two layers are more likely to occur together. During the daytime,

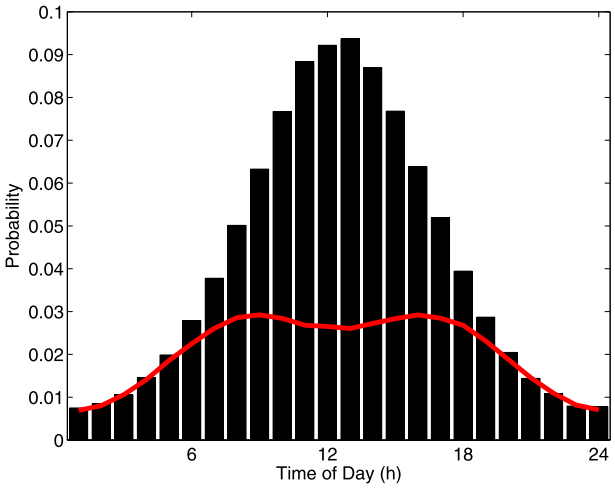

FIG. 10. Bars: Mean frequency distribution of the timing of daily maxima of $y(t) = \|\boldsymbol{\nu}(t)\|$ [Eq. (4)] with resolution $\delta = 1$ h, obtained by averaging individual distributions over all $N_{\text{base}} = 24$ base times t_0 from 0000 to 2300 [Eq. (5)]. Red curve: standard deviation of frequency distributions across base times [Eq. (6)].

the two populations in the timing of extrema (simultaneous and asynchronous) can be interpreted as reflecting variability in the strength of the LLJ from night to night. In the simplest model of LLJ dynamics, the maximum strength of the LLJ is determined by the difference between the boundary layer wind vector and the geostrophic wind vector (e.g., Thorpe and Guymer 1977) at the time when the residual and inversion layers decouple [or with the equilibrium wind vector, as suggested by van de Wiel et al. (2010)]. If the resulting inertial oscillation is of small amplitude, or unable to align with the geostrophic wind before sunrise, then the maximum LLJ wind speed will be relatively small. In such cases, maximum wind speeds can occur in the well-mixed daytime boundary layer, simultaneously at 10 and 200 m. The simultaneous occurrence of wind extrema at the two levels at any time of day will also be influenced by strong large-scale forcing, when wind speeds are large and shear-driven turbulence couples the flow at the two altitudes. The distribution of these events is expected to be uniform throughout the day, since the large-scale forcing does not itself display a marked diurnal cycle.

4. An idealized mechanistic model of the timing of wind speed extremes

To further explore the dynamical controls on the timing of daily wind speed extrema, we will consider an idealized model of the boundary layer momentum budget adapted from that discussed in Monahan et al. (2011). This earlier model, based on the Thorpe and Guymer (1977) model of LLJ dynamics, represents the daytime boundary layer as a homogeneous slab with uniform velocity. At night, this layer splits into two layers: a shallow inversion layer and a residual layer above. These two layers are uncoupled most of the time, but are occasionally coupled by an intermittent process representing episodic mixing events at the top of the inversion layer. At sunrise, the two layers merge and the process repeats. At all times, the winds are subject to pressure gradient and Coriolis forces; the daytime layer and the lowermost nocturnal layer are also subject to surface drag.

The sharp discontinuities at sunrise and sunset in the model of Monahan et al. (2011) produce impulsive responses in the winds at these times, resulting in extreme winds that tend to be strongly synchronized with the separation and merger of the two nocturnal layers. In reality, the development of the nocturnal inversion layer and the growth of the daytime convective boundary layer—while relatively rapid—are smooth transitions. The boundary layer momentum budget model was modified accordingly, to account for the smooth transitions between daytime and nighttime boundary layer structures. As well, the lower of the nocturnal boundary layers is reinterpreted as the actively turbulent layer in which shear production overcomes buoyant consumption of turbulence kinetic energy (rather than as the inversion layer). A schematic illustration of the evolution of the boundary layer in the model is presented in Fig. 13. Just before sunrise, the lowermost layer has specified depth H_S. Above this is the residual layer with depth H_R. At sunrise, buoyant generation of turbulence allows the lower layer to grow into the residual layer above, entraining fluid as it does so. When it reaches a specified thickness, H_C, it stops growing but continues to turbulently exchange momentum with the fluid above (which is assumed to be in geostrophic balance). At dusk, the turbulent layer depth decreases uniformly toward the fixed minimum depth H_S. The model equations are presented in detail in the appendix.

The mean diurnal cycle of wind speed simulated by this model in each of the two layers is presented in Fig. 14, along with the mean JAS diurnal cycle observed at Cabauw. In broad terms, the model captures the general features of the observed mean diurnal cycle, although it somewhat overestimates the speed. The effect of the smoothed dawn and dusk transitions is evident in the relatively smooth evolution of the modeled wind speeds. The distributions of the maximum 24-h wind speeds at 10 and 200 m are shown in Fig. 15, along with the 95th percentiles of the wind speeds from 2-day windows. In their broad features, these capture the main features of the extreme timing distribution of observed winds (Fig. 11). The local peaks in the timing of extreme

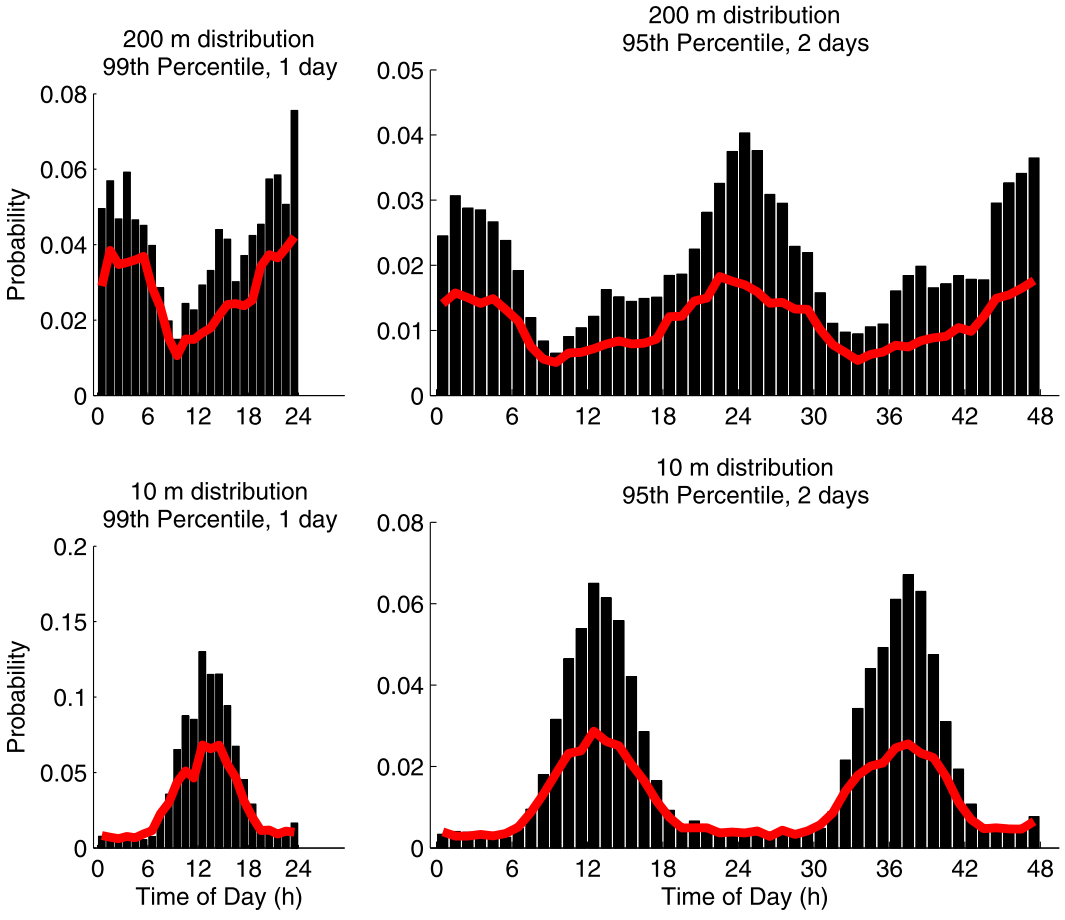

FIG. 11. (left) Mean (bars) and standard deviation (red curve) across the frequency distributions of daily maximum (top) 200-m and (bottom) 10-m wind speeds computed for base times t_0 = 0000 to 2350. (right) As at left, but for wind speeds exceeding the 95th percentile in 2-day windows.

10-m winds result from remaining artificial, abrupt changes in the modeled dynamics, which are not characteristic of the real atmospheric boundary layer. The observed daytime secondary maximum in the timing of 200-m wind extremes during the day is also absent; the low-level jets produced by the model are more regular than those in the observed winds, so the maximum wind speed in the upper layer almost always occurs at night. The joint distribution of the timing of extreme wind speeds in the upper and lower layers, calculated as in Fig. 12, is displayed in Fig. 16. Again, the features of the observed joint distribution are broadly captured. The different populations described in the previous section are evident, although the population in which the extrema are synchronized at the same time of day is underpopulated in the model (particularly during the day). When the intermittent mixing of the inversion and residual layers at night is turned off, the synchronized nocturnal population vanishes. That is, wind speed extrema at 10 and 200 m are not found to occur simultaneously at night in the absence of this episodic coupling. This result is consistent with the physical interpretation of this population presented in the previous section.

While the model's representation of the timing of extrema is not in exact agreement with the observed distribution, and despite the fact that it is highly idealized, it captures the qualitative features of observations. These results provide evidence that the physical mechanisms identified in the previous section, which make up the basic elements of the model, are in fact responsible for producing these populations.

5. Discussion and conclusions

This study has considered the timing of daily near-surface wind speed extrema in 11 years of 10-min resolution observations from the 213-m-tall tower at Cabauw, the Netherlands. To carry out this analysis, it was necessary to distinguish physically driven variations in the likelihood of the occurrence of extrema from the "edge

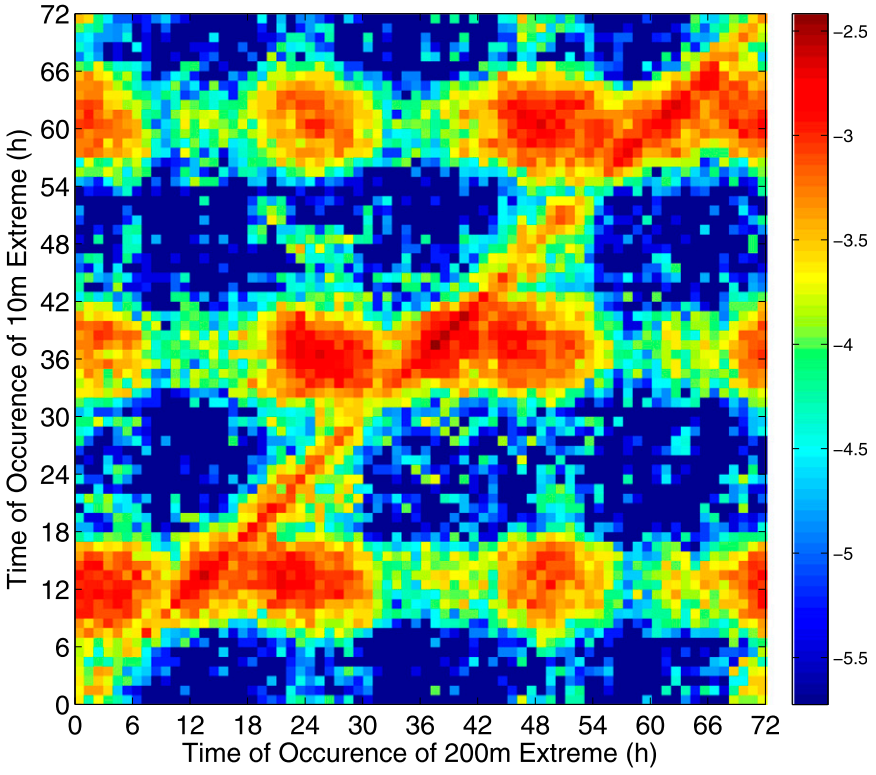

FIG. 12. Base-10 logarithm of the mean joint distribution of the timing of wind speeds exceeding the 95th percentile at 10 and 200 m in a 3-day window, averaged across all base times t_0 = 0000 to 2350.

effects'' causing the probability of occurrence to concentrate around the beginning and end of the day. The first of these, resulting from intrinsic, astronomically forced nonstationarities in the time series, is independent of how the day is defined, while the second varies with changes in the base hour used to separate one day from the next. It was demonstrated that by averaging across frequency distributions of the timing of the occurrence of extrema calculated for each possible base time, the edge effect can to a large extent be filtered out and the intrinsic, physically driven nonstationarity emphasized.

For the winds at Cabauw, it was found that wind speed extrema in the bottom few tens of meters of the atmosphere are most likely to occur in the late morning/early afternoon. At 200 m, extreme wind speeds are most likely to occur at night—although the probability of wind speed extremes occurring during the afternoon or early evening at these altitudes is not negligible. Consideration of the joint distribution of the timing of wind speed extremes at 10 and 200 m demonstrated that most often these do not occur simultaneously, with the 10-m extremes occurring during the day and the 200-m extremes at night. However, there are occasions in which the extremes occur together at both altitudes. The simultaneous occurrence during the day was interpreted as resulting from weakly developed low-level jets on the preceding and following nights. At night, the simultaneous occurrence was interpreted as resulting from the episodic coupling of the surface inversion layer and the residual layer above that has been documented in previous studies (e.g., Monahan et al. 2011; He et al. 2012). The structure of the timing of wind speed extrema at these altitudes was qualitatively simulated by an idealized stochastic model of the boundary layer momentum budget.

Previous studies that considered the timing of extremes of time series within specified windows (e.g., Leadbetter

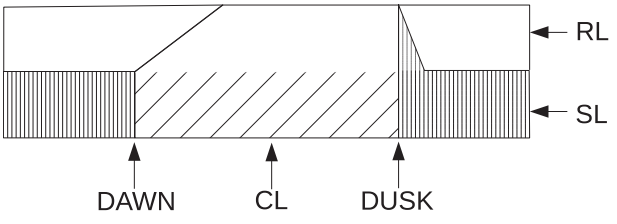

FIG. 13. Schematic diagram of the evolution of the boundary layer in the idealized momentum budget model (described in detail in the appendix). SL: turbulent surface layer; RL: residual layer; CL: convective layer.

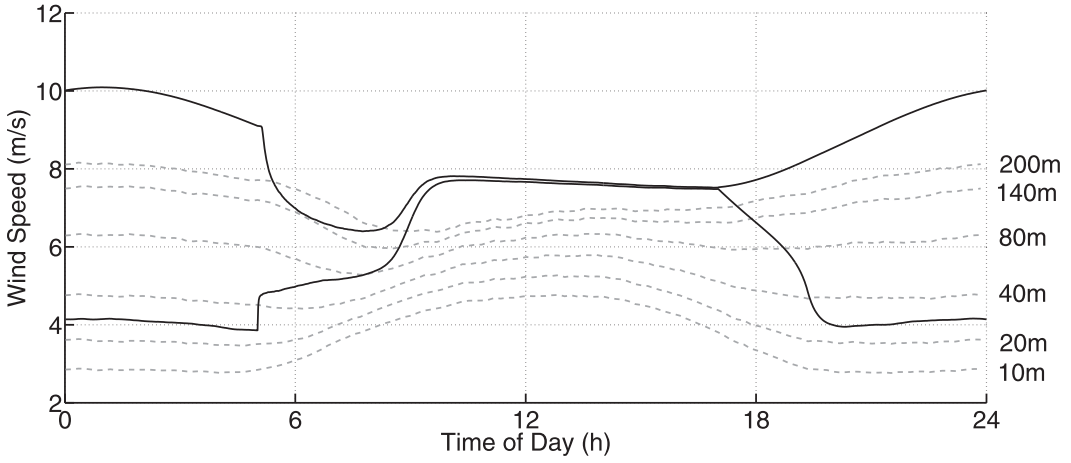

FIG. 14. Mean diurnal cycle of 10-m (lower solid curve) and 200-m (upper solid curve) modeled winds, superimposed on the observed JJA evolution of wind speeds at Cabauw (dashed; with levels as in Fig. 1). Note that the modeled mean wind speeds are not exactly equal during the day because the actively turbulent layer does not reach 200 m every day as a result of variability in the entrainment velocity $w_e(t)$ [Eq. (A10)].

et al. 1983; Coakley 2000; Samorodnitsky and Shen 2013a,b) demonstrated the existence of the edge effect but did not address strategies to filter it in order to enhance the physically driven signal present in the inherent nonstationarities. The present study has demonstrated that this filtering can be carried out with a simple averaging procedure. Of course, if the inherent nonstationarity is weak, then sufficiently long time series must be available

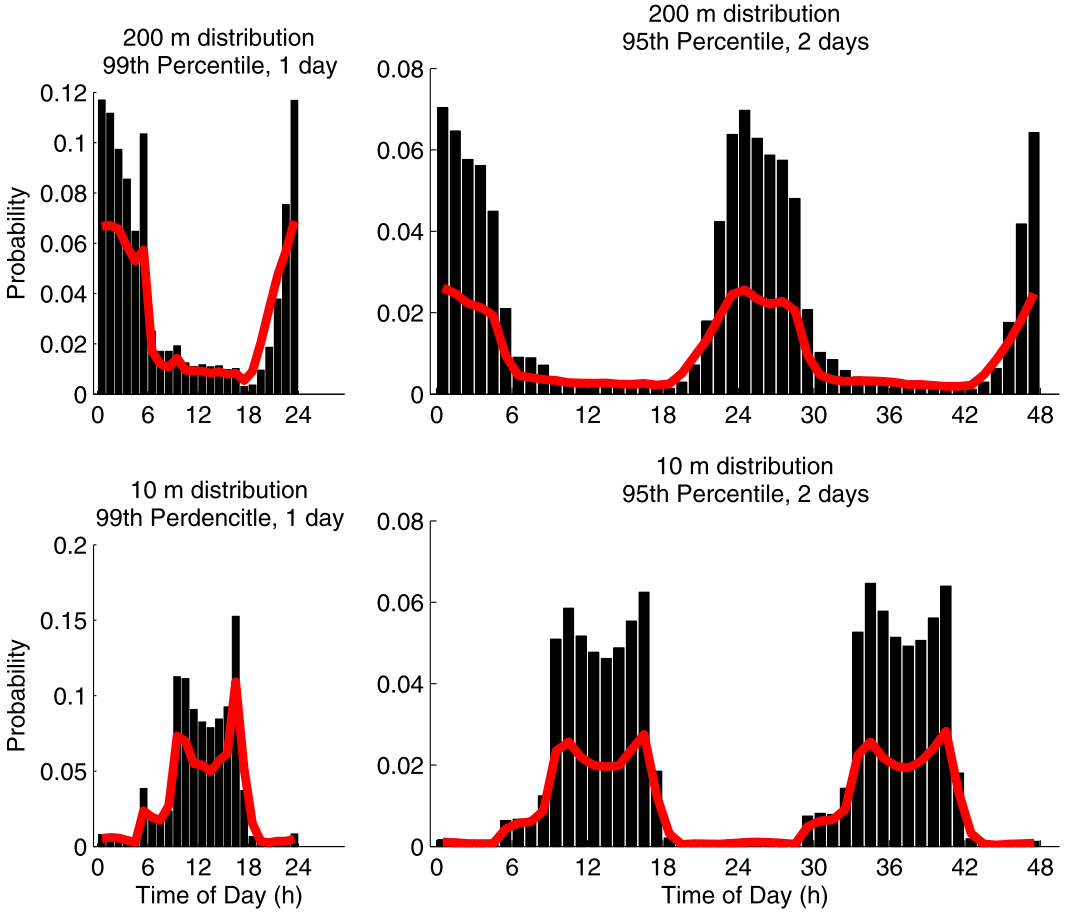

FIG. 15. As in Fig. 11, but for winds simulated by the idealized momentum budget model.

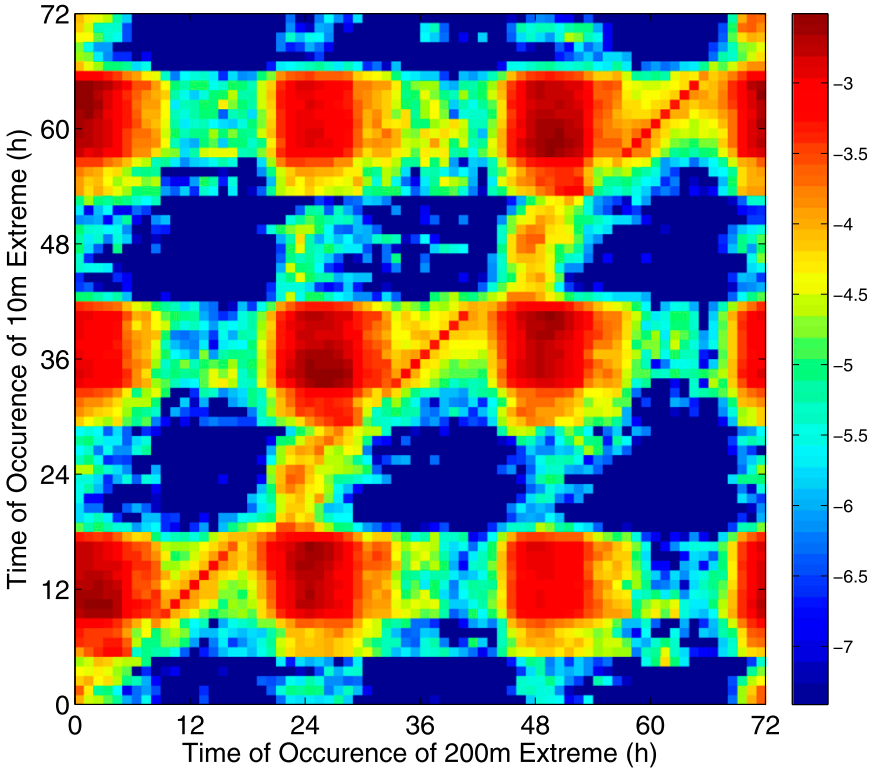

FIG. 16. As in Fig. 12, but for winds simulated by the idealized momentum budget model.

for the signal to emerge from the sampling variability in the frequency distributions. The long duration of the dataset available from the tower observations at Cabauw is a fundamental reason why it is so useful.

The present analysis has considered the timing of daily wind speed extrema without accounting for other factors that may influence the occurrence of these extremes. For example, the presence of low clouds has been shown to strongly influence the diurnal cycle of the probability density function (and in particular the tails) of near-surface winds (He et al. 2013). A more refined analysis would consider the influences of variability of cloud cover and large-scale geostrophic winds on the timing of extrema. Such an analysis is an interesting direction of future study.

This study has demonstrated that the simple method of determining the timing of maxima (and more generally, extrema) within specified time windows can be used to determine physically driven, inherent nonstationarities in this timing despite the tendency of these extrema to cluster at the beginning and end of the window—if an appropriate averaging of distributions across base times is used. Although we have introduced this strategy in the context of the daily timing of near-surface wind speed extremes, the approach is generic and can be applied to the study of the extreme timing of any other climate variable. The use of this averaging strategy to investigate the timing of extrema at other locations, or for different variables (e.g., wind shear, temperature, precipitation) or window lengths (e.g., weekly, monthly, annual), could produce interesting directions of future study.

Acknowledgments. The authors thank Alex Cannon for helpful discussions, Fred Bosveld of KNMI for providing the surface geostrophic wind data, and the Cabauw Experimental Site for Atmospheric Research (Cesar) for providing the tower observations. We also thank three anonymous reviewers for their helpful comments. RF was supported in this research by the Natural Sciences and Engineering Research Council (NSERC) of Canada CREATE Project on Interdisciplinary Climate Science. AM further acknowledges support from the NSERC Discovery Grant program.

APPENDIX

Idealized Boundary Layer Wind Model

When the daytime turbulent layer is fully developed and of depth H_C, its momentum budget is represented with a single bulk layer of velocity $\mathbf{U}_C$:

$$\frac{d\mathbf{U}_C}{dt} = -\hat{k}f \times (\mathbf{U}_C - \mathbf{U}_G) - \frac{w_e(t)}{H_C}(\mathbf{U}_C - \mathbf{U}_G) - \frac{c_C}{H_C}\mathbf{U}_C\|\mathbf{U}_C\|, \tag{A1}$$

where $\mathbf{U}_G$ is the geostrophic velocity, $w_e(t)$ is the (time dependent) entrainment velocity, f is the Coriolis parameter, and c_C is the drag coefficient. A basic assumption of the model is that the statistics of variability in near-surface winds can be modeled in terms of the statistics of the large-scale free-tropospheric driving processes manifested through the pressure gradient force. Accordingly, the geostrophic winds are modeled as a red noise process with a mean $\overline{\mathbf{U}_G} = (\overline{U}_G, 0)$, standard deviation σ, and autocorrelation time τ:

$$\mathbf{U}_G = \overline{\mathbf{U}_G} + \boldsymbol{\eta}, \tag{A2}$$

where the vector $\boldsymbol{\eta}$ is described by the SDE

$$\dot{\boldsymbol{\eta}} = \frac{-\boldsymbol{\eta}}{\tau} + \sigma\sqrt{\frac{2}{\tau}}\dot{\mathbf{W}}_g, \tag{A3}$$

with $\dot{\mathbf{W}}_g$ being a vector of uncorrelated Gaussian white noise processes (e.g., Gardiner 1997). The parameters of $\mathbf{U}_G$ are set to match those of the observed geostrophic wind at Cabauw.

At dusk, the single mixed layer splits into a surface shear-driven turbulent layer and a residual layer with respective velocities $\mathbf{U}_S$ and $\mathbf{U}_R$, such that at the time t_n of this transition

$$\mathbf{U}_S(t_n) = \mathbf{U}_R(t_n) = \mathbf{U}_S(t_n). \tag{A4}$$

The equations of motion of these two layers are given by

$$\frac{d\mathbf{U}_R}{dt} = -\hat{k}f \times (\mathbf{U}_R - \mathbf{U}_G) - \frac{Z(t)}{h_R}(\mathbf{U}_R - \mathbf{U}_S) \tag{A5}$$

and

$$\frac{d\mathbf{U}_S}{dt} = -\hat{k}f \times (\mathbf{U}_S - \mathbf{U}_G) - \frac{w_e(t) + Z(t)}{h_S}(\mathbf{U}_S - \mathbf{U}_R) - \frac{c_s}{h_S}\mathbf{U}_S\|\mathbf{U}_S\|. \tag{A6}$$

By definition,

$$-\frac{dh_R}{dt} = \frac{dh_S}{dt}. \tag{A7}$$

As the turbulent layer grows after dawn, we take

$$\frac{dh_S}{dt} = w_e. \tag{A8}$$

As this turbulent layer grows, its velocity tendency is influenced by the entrainment of fluid from above, while the residual layer momentum budget is unaffected by this process. Once $h_c = H_C$, the residual layer is removed and it is assumed that large-scale subsidence keeps the height of the actively turbulent boundary layer constant. In the dusk transition, h_S linearly decreases from H_C to H_S over the time T_{trans}, and $w_e = 0$.

The entrainment velocity is modeled using a combination of shear and stratification measures. For simplicity, these are considered to be uncorrelated. As in He et al. (2012), the turbulence kinetic energy (TKE) is assumed to be horizontally homogeneous with a budget that is in local equilibrium. Neglecting transport processes and using a first-order flux gradient closure, the TKE budget can be expressed as

$$K_m(S_x^2 + S_y^2) - \mathrm{Pr}^{-1}K_m N^2 = \epsilon, \tag{A9}$$

where S_x and S_y are the zonal and meridional wind shear components, respectively, K_m is the eddy viscosity, Pr is the turbulent Prandtl number, N^2 is the Brunt–Väisälä frequency, and ϵ is the dissipation rate. With the standard assumptions that $K_m \sim (\mathrm{TKE})^{1/2}$ and $\epsilon \sim (\mathrm{TKE})^{3/2}$, the entrainment velocity (which differs from K_m by a characteristic length scale L, which we assume to be constant) can be written as

$$w_e = \begin{cases} C_e L[(S_x^2 + S_y^2) - \mathrm{Pr}^{-1}N^2]^{1/2} & \text{if} \quad S_x^2 + S_y^2 \geq \mathrm{Pr}^{-1}N^2 \\ 0 & \text{otherwise} \end{cases}, \tag{A10}$$

where C_e is a scaling constant. For simplicity, we assume a fixed turbulent Prandtl number Pr = 1.35. Note that the use of a constant value for Pr imposes a cutoff on turbulent mixing at a finite gradient Richardson number. We estimate S_x and S_y as

$$S_x = U_{G_x}/L \tag{A11}$$

and

$$S_y = U_{G_y}/L. \tag{A12}$$

The evolution of the Brunt–Väisälä frequency is modeled as containing both deterministic and random components:

$$N^2 = \nu(t) + F(t). \tag{A13}$$

The function $F(t)$ represents the average effects of the diurnal cycle on stratification; we have modeled it as

$$F(t) = F_0 + F_0 \tanh(0.05s - 20/3), \tag{A14}$$

where $s = t \pmod{24\,\text{h}}$ is the time of day (hours since midnight). The form of $F(t)$ was chosen in order to represent the smooth transition in stratification over the course of the day due to surface heating. The random process $\nu(t)$, which represents the variable influence of weather on the stratification, is also represented as a red-noise process:

$$\frac{d\nu}{dt} = \frac{-\nu}{\tau_\nu} + \sigma_\nu \sqrt{\frac{2}{\tau_\nu}} \dot{\mathbf{W}}_\nu. \tag{A15}$$

The quantity $Z(t)$ in Eqs. (A5) and (A6) models the effect of intermittent turbulent mixing in the stably stratified boundary layer, represented here (as in Monahan et al. 2011) as a stochastic process:

$$Z(t) = Z_o \frac{|x|^n}{\mathbf{E}\langle |x|^n \rangle}, \tag{A16}$$

with x given by

$$\frac{dx}{dt} = \frac{-x}{\tau_x} + \sqrt{\frac{2}{\tau_x}} \dot{\mathbf{W}}_z. \tag{A17}$$

During the daytime, when there is buoyant generation of TKE and $w_e(t) \neq 0$ (in general), we take $Z(t) = 0$.

$$\mathbf{U}_{200} = \begin{cases} \mathbf{U}_R, & 200\,\text{m} \geq h_S + h_I \\ \mathbf{U}_I = \dfrac{\mathbf{U}_R - \mathbf{U}_S}{h_I}(200\,\text{m} - h_S) + \mathbf{U}_S & h_S + h_I > 200\,\text{m} > h_S \\ \mathbf{U}_S, & h_S \geq 200\,\text{m} \\ \mathbf{U}_C, & h_s = H_C \end{cases}. \tag{A19}$$

By construction, the 10-m altitude is always within the lowest model layer.

TABLE A1. Parameter values used for the idealized stochastic boundary layer momentum budget.

Parameter	Units	Value
dt	s	60
f	s^{-1}	1.14×10^{-4}
c_C	—	16×10^{-3}
H_C	m	250
H_R	m	200
H_S	m	50
H_I	m	10
T_{trans}	h	2
$\overline{\mathbf{U}_G}$	m s^{-1}	8.5
σ	m s^{-1}	5
τ	h	48
Ce	—	0.002
L	m	50
Pr	—	1.35
F_o	s^{-2}	3600
τ_ν	h	48
σ_ν	s^{-2}	5
τ_x	h	3
Z_o	—	5×10^{-3}

Diurnal drag variation is introduced by the equation

$$c_s = 0.1 c_c, \tag{A18}$$

which is based on empirical observations made at a site similar to Cabauw (Miao and Ji 1996).

While this model represents the momentum budgets of slab layers of varying thickness, the observed winds are observed at fixed altitudes. To minimize jump discontinuities in the modeled wind at any altitude as the layer interface passes, a narrow interface layer of thickness h_I is added between the bottom of the residual layer and the top of the growing convective layer during the daytime transition. This layer does not influence the dynamics; it is simply results in a continuous transition between the vector winds in the two layers. Specifically, the wind at 200 m is given by

Values of the model parameters used in this study are presented in Table A1.

REFERENCES

Arya, S. P., 2001: *Introduction to Micrometeorology.* Academic Press, 420 pp.

Baas, P., F. Bosveld, H. K. Baltink, and A. Holtslag, 2009: A climatology of low-level jets at Cabauw. *J. Appl. Meteor. Climatol.,* **48,** 1627–1642, doi:10.1175/2009JAMC1965.1.

——, ——, G. Lenderink, E. van Meijgaard, and A. Holtslag, 2010: How to design single-column model experiments for comparison with observed nocturnal low-level jets. *Quart. J. Roy. Meteor. Soc.,* **136,** 671–684, doi:10.1002/qj.592.

Barthelmie, R., B. Grisogono, and S. Pryor, 1996: Observations and simulations of diurnal cycles of near-surface wind speeds over land and sea. *J. Geophys. Res.,* **101,** 21 327–21 337, doi:10.1029/96JD01520.

Burton, T., N. Jenkins, D. Sharpe, and E. Bossanyi, 2011: *Wind Energy Handbook.* Wiley, 742 pp.

Coakley, K. J., 2000: The warmest day of any week tends to occur on the first or last day of that week. *Bull. Amer. Meteor. Soc.,* **81,** 273–283, doi:10.1175/1520-0477(2000)081<0273:TWDOAW>2.3.CO;2.

Dai, A., and C. Deser, 1999: Diurnal and semidurnal variations in global surface wind and divergence fields. *J. Geophys. Res.,* **104,** 31 109–31 125, doi:10.1029/1999JD900927.

Gardiner, C. W., 1997: *Handbook of Stochastic Methods for Physics, Chemistry, and the Natural Sciences.* Springer, 442 pp.

He, Y., A. H. Monahan, C. G. Jones, A. Dai, S. Biner, D. Caya, and K. Winger, 2010: Probability distributions of land surface wind speeds over North America. *J. Geophys. Res.,* **115,** D04103, doi:10.1029/2008JD010708.

——, N. A. McFarlane, and A. H. Monahan, 2012: The influence of boundary layer processes on the diurnal variation of the climatological near-surface wind speed probability distribution over land. *J. Climate,* **25,** 6441–6458, doi:10.1175/JCLI-D-11-00321.1.

——, A. H. Monahan, and N. A. McFarlane, 2013: Diurnal variations of land surface wind speed probability distributions under clear-sky and low-cloud conditions. *Geophys. Res. Lett.,* **40,** 3308–3314, doi:10.1002/grl.50575.

Kloeden, P. E., and E. Platen, 1992: *Numerical Solution of Stochastic Differential Equations.* Springer Verlag, 632 pp.

Leadbetter, M., G. Lindgren, and H. Rootzen, 1983: *Extremes and Related Properties of Random Sequences and Processes.* Springer Verlag, 336 pp.

Miao, M., and J. Ji, 1996: Study on diurnal variation of bulk drag coefficient over different land surfaces. *Meteor. Atmos. Phys.,* **61,** 217–224, doi:10.1007/BF01025707.

Monahan, A. H., 2012: The temporal autocorrelation structure of sea surface winds. *J. Climate,* **25,** 6684–6700, doi:10.1175/JCLI-D-11-00698.1.

——, 2014: Wind speed probability distribution. *Encyclopedia of Natural Resources,* Y. Wang, Ed., Taylor and Francis, in press.

——, Y. He, N. McFarlane, and A. Dai, 2011: The probability distribution of land surface wind speeds. *J. Climate,* **24,** 3892–3909, doi:10.1175/2011JCLI4106.1.

Samorodnitsky, G., and Y. Shen, 2013a: Is the location of the supremum of a stationary process nearly uniformly distributed? *Ann. Probab.,* **41,** 3494–3517, doi:10.1214/12-AOP787.

——, and ——, 2013b: Intrinsic location functionals of stationary processes. *Stoch. Proc. Appl.,* **123,** 4040–4064, doi:10.1016/j.spa.2013.06.008.

Stull, R. B., 1997: *An Introduction to Boundary Layer Meteorology.* Kluwer, 666 pp.

Thorpe, A. J., and T. H. Guymer, 1977: The nocturnal jet. *Quart. J. Roy. Meteor. Soc.,* **103,** 633–653, doi:10.1002/qj.49710343809.

van de Wiel, B., A. Moene, G. Steeneveld, P. Baas, F. Bosveld, and A. Holtslag, 2010: A conceptual view on inertial oscillations and nocturnal low-level jets. *J. Atmos. Sci.,* **67,** 2679–2689, doi:10.1175/2010JAS3289.1.

van Ulden, A., and J. Wieringa, 1996: Atmospheric boundary layer research at Cabauw. *Bound.-Layer Meteor.,* **78,** 39–69, doi:10.1007/BF00122486.